

Structural changes of Nd- and Ce-doped ammonium diuranate during the conversion to $U_{1-y}Ln_yO_{2\pm x}$

Christian Schreinemachers^{1,2,3}, Gregory Leinders¹, Renaud Podor⁴, Nicolas Clavier⁴, Giuseppe Modolo³, Marc Verwerft¹, Koen Binnemans² and Thomas Cardinaels^{1,2}

¹ Belgian Nuclear Research Centre (SCK CEN), Institute for Nuclear Materials Science, Mol, Belgium

² KU Leuven, Department of Chemistry, Heverlee, Belgium

³ Forschungszentrum Jülich GmbH, Institute of Energy and Climate Research (IEK-6), Jülich, Germany

⁴ ICSM, Univ Montpellier, CEA, CNRS, ENSCM, Bagnols-sur-Cèze, France

Nuclear Fuel Cycle: A Chemistry Conference (NFC3) | May 4-5, 2021

NFC3

KU LEUVEN

sck cen



JÜLICH
Forschungszentrum

Outline

1. Introduction

- 1.1 Nuclear fuel cycle
- 1.2 P&T strategy
- 1.3 Sphere-Pac fuel
- 1.4 Internal gelation

2. Particle fabrication

- 2.1 Schematic overview
- 2.2 Gelation parameter
- 2.3 Results

3. Decomposition in air

- 3.1 Conversion of ADU to α -U₃O₈
- 3.2 Conversion of *Ln*-doped ADU particles
- 3.3 Characterisation of calcination products


4. Reductive sintering

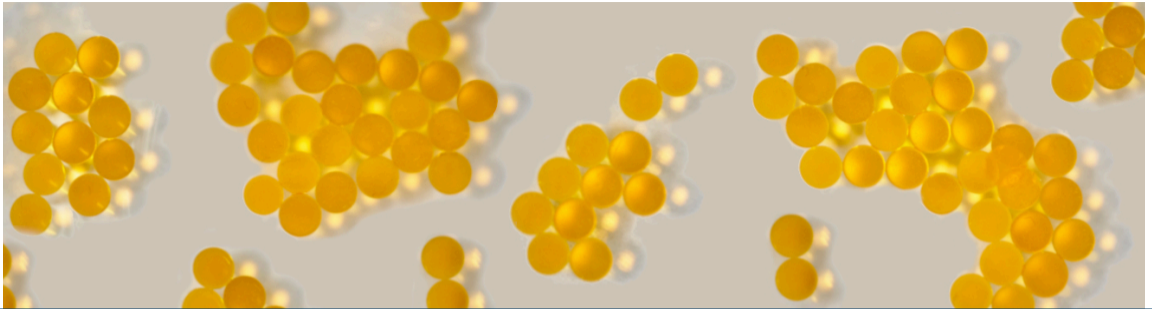
- 4.1 *In-situ* characterisation
- 4.2 Characterisation of sintered products

5. Conclusions

6. References

DOI [10.5281/zenodo.4727052](https://doi.org/10.5281/zenodo.4727052)

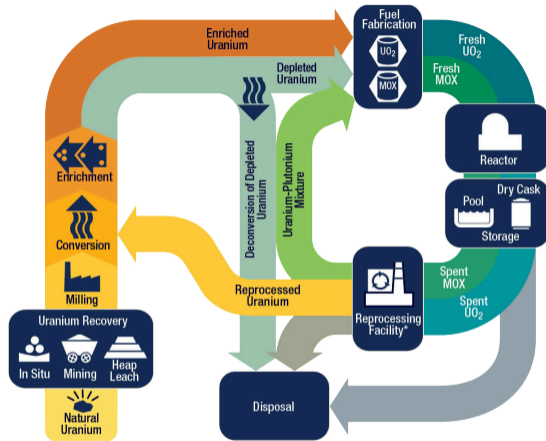
This work is licensed under a Creative Commons "Attribution-NonCommercial 4.0 International" license. 



Part I: Introduction

(Nuclear Fuel Cycle, Partitioning & Transmutation, Sphere-Pac fuel, Internal gelation)

Nuclear fuel cycle and composition of spent fuel



Scheme taken from the US Nuclear Regulatory Commission - The Nuclear Fuel Cycle
 (source: <https://www.flickr.com/photos/nrcgov/36631029882>, license:)

Fission products
Activation products
Major actinides
Minor actinides

1A																	2A											3A	4B	5A	6A	7A	8A																
1	H																2	He										3	4	5	6	7	8	9	10														
3	Li																4	Be										5	6	7	8	9	10	11															
11	Na																12	Mg										13	14	15	16	17	18	19															
19	K																20	Ca																21	22	23	24	25	26	27	28	29	30	31	32	33	34	35	36
37	Rb																38	Sr																39	40	41	42	43	44	45	46	47	48	49	50	51	52	53	54
55	Cs																56	Ba																57	58	59	60	61	62	63	64	65	66	67	68	69	70	71	72
87	Fr																88	Ra																89	90	91	92	93	94	95	96	97	98	99	100	101	102	103	104
105	Nh																106	Fl																107	108	109	110	111	112	113	114	115	116	117	118	119	120	121	122
123	Uu																124	Uu																125	126	127	128	129	130	131	132	133	134	135	136	137	138	139	140
Lanthanides																	57	58	59	60	61	62	63	64	65	66	67	68	69	70	71																		
Actinides																	89	90	91	92	93	94	95	96	97	98	99	100	101	102	103																		

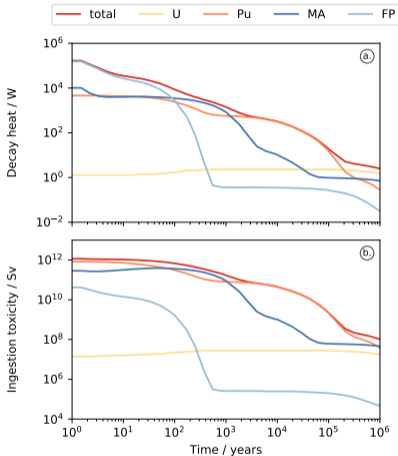
Scenarios currently applied

- Once-through fuel cycle: direct disposal
- Twice-trough fuel cycle: reprocessing

Partitioning and transmutation (P&T)

- Advanced fuel cycle: minor actinide recycling

Properties of spent nuclear fuel

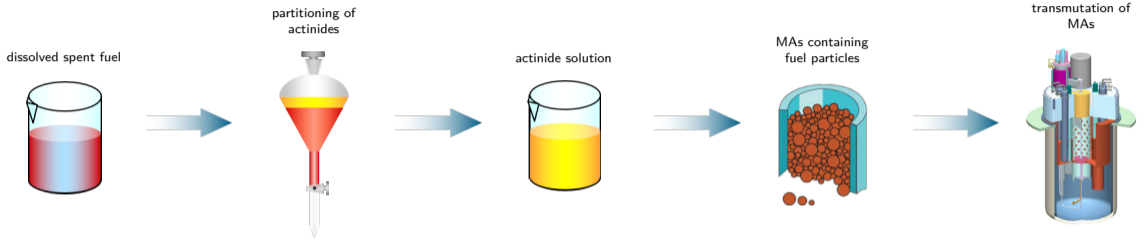


initial heavy metal mass of 20 t, enriched to 4.6 wt% in $^{235}_{92}\text{U}$,
burn-up of 50 MWd/kg and 5 years use in a PWR

- FPs are most significant for shorter term
- Pu and MAs dominate the long-term heat generation and radiotoxicity
- a removal of Pu leads to a heat and radiotoxicity reduction ('twice trough' fuel cycle)
- an additional separation of the MAs results in a further reduction ('advanced' fuel cycle)

A smaller heat emission is desired to reduce the final storage repository volume.

The partitioning and transmutation strategy

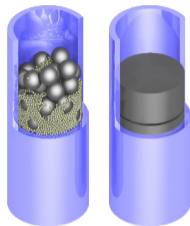


- 1 Dissolution of spent nuclear fuel in nitric acid
- 2 Partitioning of actinides from dissolved spent fuel by liquid/liquid separation processes
- 3 **Conversion of solution containing minor actinides (MAs) into nuclear fuel particles**
- 4 Transmutation of the MAs in advanced nuclear reactor systems

Advanced nuclear fuels: The Sphere-Pac fuel concept

Fuel pin filled with spherical particles of 2 or 3 different size fractions.

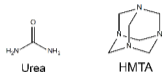
- easy fabrication in terms of remote handling
- synthesis possible with almost no formation of dust
- no need for mechanical treatment (e.g. grinding, pressing, polishing)
⇒ direct insertion of particles into the fuel pin possible
- lower smear density
- low initial thermal conductivity
- more sophisticated pin-filling procedure



Methods to prepare spherical fuel particles:

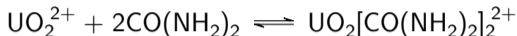
- weak acid resin process
- **sol-gel techniques** ⇒ conversion of a **liquid sol** into a **solid gel**

Sol-gel techniques: Internal gelation

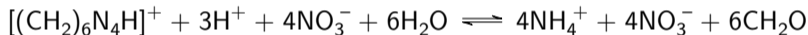


Uranyl complexation (\rightarrow) / de-complexation (\leftarrow):

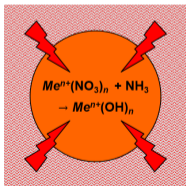
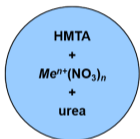
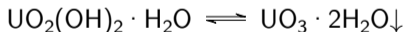
source^a



Hexamethylenetetramine (HMTA) protonation and decomposition:



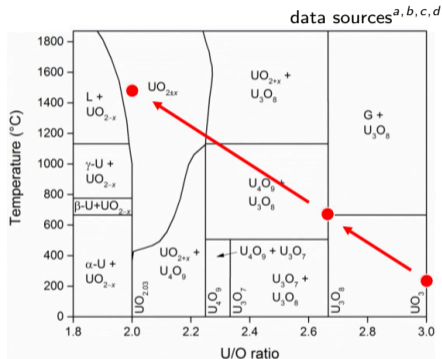
Uranyl hydrolysis:



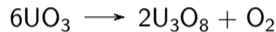
^aCollins et al. 1987. DOI: 10.1524/ract.1987.42.3.121.

Thermal treatment: Conversion of UO_3 into UO_2

U-O phase diagram



1 calcination in air:



2 sintering in reducing environment:



An oxygen potential of $\approx 420 \text{ kJ mol}^{-1}$ leads to $\text{UO}_{2\pm x}$ with $x < 0.0005$ at $1600 \text{ }^\circ\text{C}$ ^{a, b}.

^aChevalier et al. 2002. DOI: 10.1016/S0022-3115(02)00813-9.

^bLabroche et al. 2003. DOI: 10.1016/S0022-3115(02)01322-3.

^cHiggs et al. 2007. DOI: 10.1016/j.jnucmat.2006.12.050.

^dGuéneau et al. 2011. DOI: 10.1016/j.jnucmat.2011.07.033.

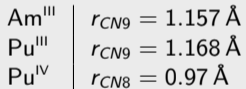
^aLindemer and Besmann. 1985. DOI: 10.1016/0022-3115(85)90334-4.

^bLeinders et al. 2015. DOI: 10.1016/j.jnucmat.2015.01.029.

Lanthanides as surrogates for actinides

To avoid the handling of radiotoxic materials, lanthanides are used to simulate actinides. They show a similar chemical behaviour and the assignment of the surrogates is based on radii and oxidation states.

actinide



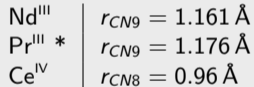
sources^{a, b}

^aShannon. 1976. DOI: 10.1107/S0567739476001551.

^bLundberg and Persson. 2016. DOI: 10.1016/j.ccr.2016.04.003.

recommended surrogate
based on ionic radii

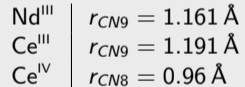
lanthanide

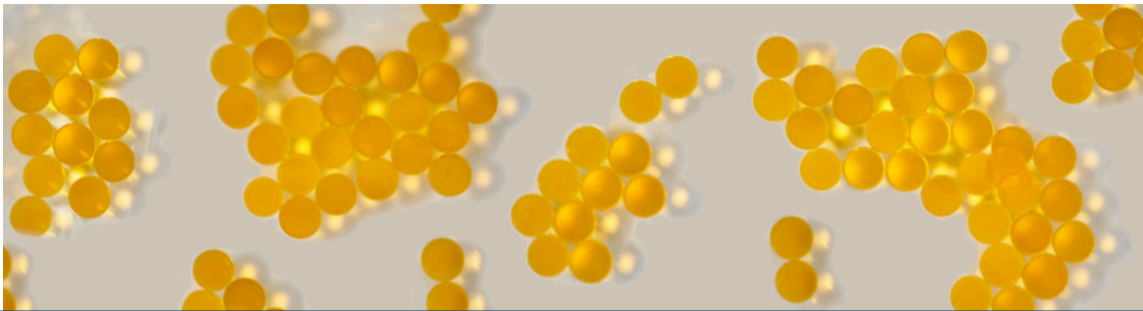


* or Nd^{III}

recommended surrogate
based on oxidation state

lanthanide





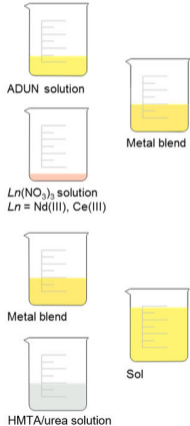
Part II: Fabrication of Nd- and Ce- doped UO_2 particles

(Metal precursors: UO_2^{2+} and Nd^{III} , Ce^{III} or Ce^{IV})

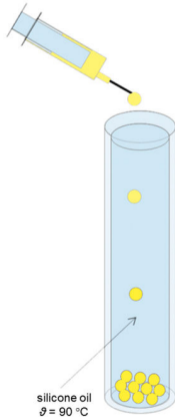
Fabrication of Nd- and Ce-doped UO_2 particles by IG

Schematic overview

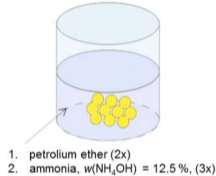
1. sol preparation



2. gelation



3. washing & ageing



4. drying in air



5. thermal treatment

a.) calcination (oxidising atmosphere)



b.) sintering (reducing atmosphere)



Fabrication of Nd- and Ce-doped UO_2 particles by IG

Gelation parameter:

- $c(M^{n+})_{\text{sol}} = 1.3 \text{ mol L}^{-1}$
- $R_{\text{urea}} = R_{\text{HMETA}} = 1.2$ $\left(R_x = \frac{c(x)}{c(M^{n+})} \right)$
- oil temperature = 90°C

Metal precursors:

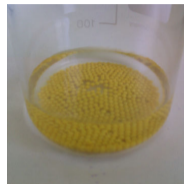
- ADUN solution, $\frac{n(\text{NO}_3^-)}{n(\text{UO}_2^{2+})} \approx 1.56$
- $\text{Nd}(\text{NO}_3)_3 \cdot 6\text{H}_2\text{O}$ solution $\rightarrow \text{Nd}^{\text{III}}$
- $\text{Ce}(\text{NO}_3)_3 \cdot 6\text{H}_2\text{O}$ solution $\rightarrow \text{Ce}^{\text{III}}$
- $(\text{NH}_4)_2[\text{Ce}(\text{NO}_3)_6]$ solid $\rightarrow \text{Ce}^{\text{IV}}$



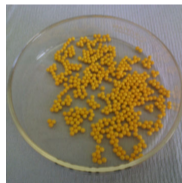
gelation



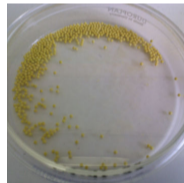
after gelation



washing & aging



before drying



after drying

Fabrication of Nd- and Ce-doped UO₂ particles by IG

Gelation behavior, trivalent dopant precursors

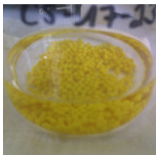
U/Nd particles

$\chi(\text{Nd}) = 5 \text{ mol}\%$

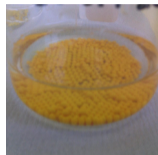
precursor: Nd^{III}
Nd(NO₃)₃ · 6H₂O



after gelation



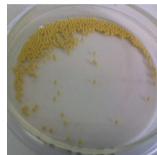
washing



aging



before drying

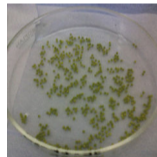
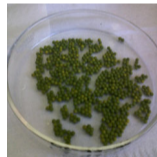
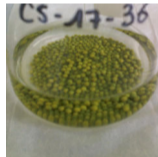
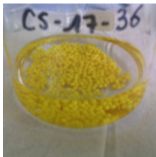


after drying

U/Ce particles

$\chi(\text{Ce}) = 5 \text{ mol}\%$

precursor: Ce^{III}
Ce(NO₃)₃ · 6H₂O



For both trivalent *Ln* dopant precursors, the gelation parameter were suitable to prepare spherical particles with dopant contents up to 30 mol%.

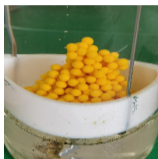
Fabrication of Nd- and Ce-doped UO_2 particles by IG

Gelation behavior, tetravalent dopant precursor

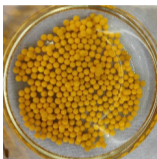
U/Ce particles

$\chi(\text{Ce}) = 5 \text{ mol}\%$

precursor: Ce^{IV}
 $(\text{NH}_4)_2[\text{Ce}(\text{NO}_3)_6]$



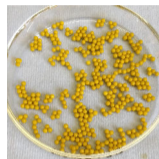
after gelation



washing



aging



before drying



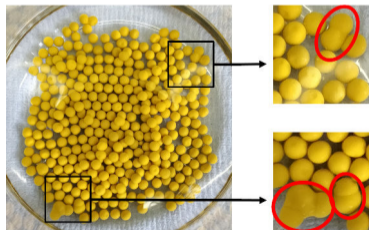
after drying

$\chi(\text{Ce})$: 10 mol% \rightarrow minor agglomeration of particles

$\chi(\text{Ce})$: 15 mol% and 20 mol% \rightarrow no spherical shape obtained

Gelation parameter suitable to prepare spherical particles
with Ce contents up to 10 mol% (Ce^{IV} precursor).

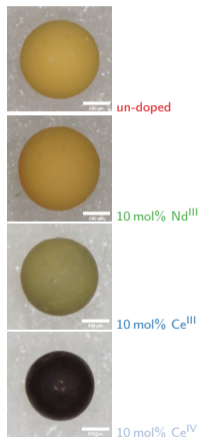
\Rightarrow



Characterisation of dried particles

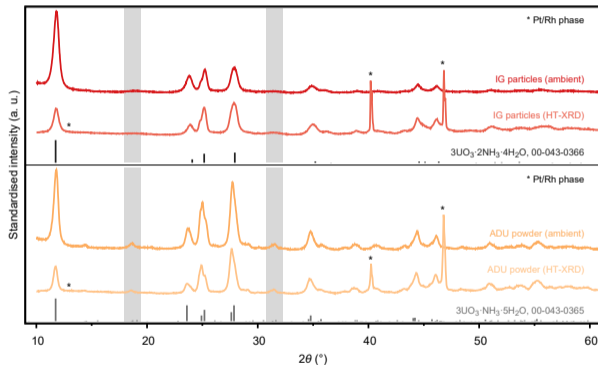
ICP-MS, OM: Particle properties

dopant precursor	$\chi(\text{dopant})_{\text{aimed}}$ / mol%	$\chi(\text{dopant})_{\text{particle}}$ / mol%	m_{dried} / mg	d_{dried} / mm	aspect ratio
–	0		3.5(3)	1.51(3)	1.04
Nd ^{III}	5	5.3(7)	3.8(6)	1.57(2)	1.03
	10	11(1)	3.6(6)	1.54(2)	1.03
	15	16(2)	5.6(6)	1.89(4)	1.02
	20	22(3)	4.5(6)	1.58(7)	1.04
	25	25(3)	6.5(5)	1.79(8)	1.07
	30	30(3)	5.5(3)	1.59(2)	1.03
Ce ^{III}	5	5.1(7)	3.2(3)	1.36(3)	1.02
	10	10(1)	3.7(3)	1.39(2)	1.01
	15	16(2)	3.8(2)	1.37(6)	1.02
	20	21(3)	3.7(2)	1.34(7)	1.05
	25	25(3)	5.6(8)	1.57(4)	1.02
	30	31(3)	5(2)	1.53(3)	1.04
Ce ^{IV}	5	4.8(7)	3.7(8)	1.30(2)	1.02
	10	10(1)	3.8(3)	1.28(2)	1.12
	15	14(2)			
	20	20(2)			



Characterisation of dried material

XRD: un-doped ADU particles and ADU powder



Solid NH₃ – UO₃ – H₂O phases^a:

- I UO₃ · 2H₂O (322.06 g mol⁻¹)
- II 3UO₃ · NH₃ · 5H₂O (321.73 g mol⁻¹)
- III 2UO₃ · NH₃ · 3H₂O (321.57 g mol⁻¹)
- IV 3UO₃ · 2NH₃ · 4H₂O (321.40 g mol⁻¹)

Compounds IV and III are hygroscopic and unstable: IV converts into III, and III into II.

- **ADU particles:** 3UO₃ · 2NH₃ · 4H₂O (IV)
- **ADU powder:** 3UO₃ · NH₃ · 5H₂O (II)

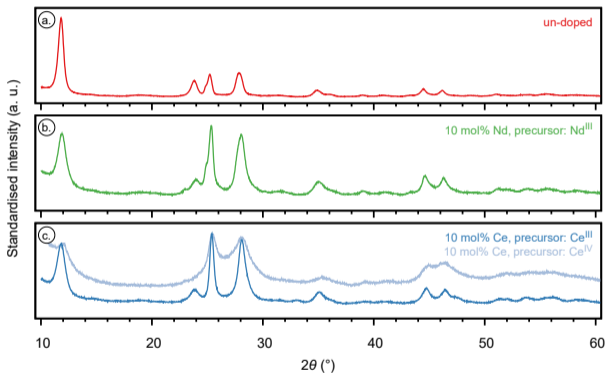
XRD references^b

^aCordfunke. 1962. DOI: 10.1016/0022-1902(62)80184-5.

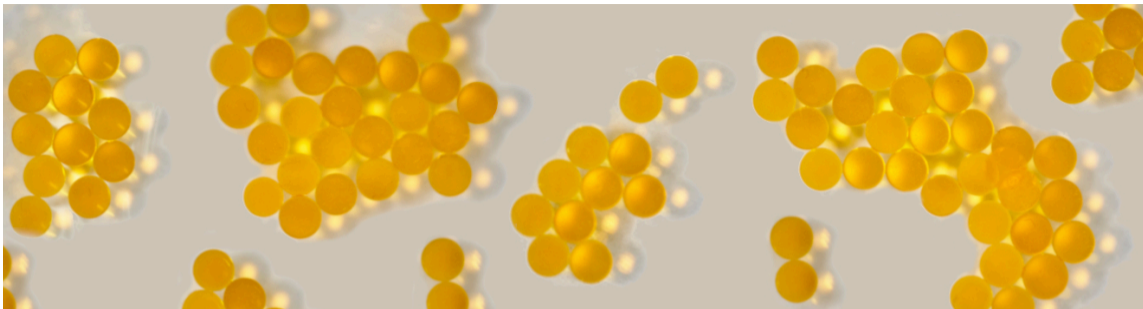
^bDebets and Loopstra. 1963. DOI: 10.1016/0022-1902(63)80027-5.

Characterisation of dried particles

XRD: un-doped and *Ln*-doped compositions (10 mol%)



- un-doped material (a) identified as $3\text{UO}_3 \cdot 2\text{NH}_3 \cdot 4\text{H}_2\text{O}$
- XRD pattern of Nd-doped gel (b) comparable to un-doped material (a), no additional reflections occur
- pattern of gel prepared with Ce^{III} (c) comparable to pattern of Nd-doped gel, indications for large fractions of an amorphous phase for Ce^{IV} particles

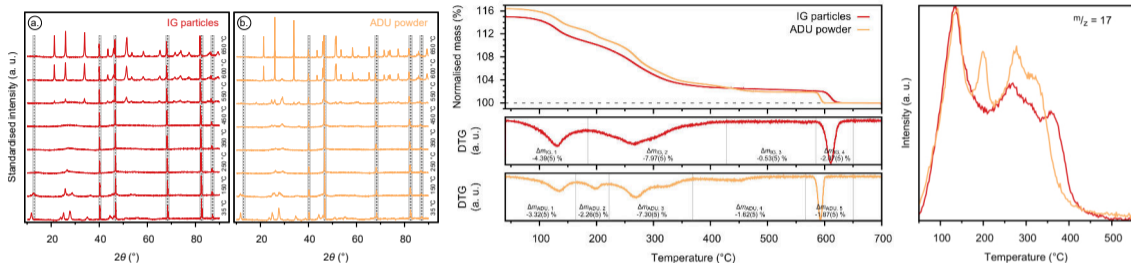


Part III: Decomposition in air

(ADU powder, ADU particles, *Ln*-doped ADU particles)

Decomposition of ADU particles and ADU powder in air

HT-XRD, TGA and EGA-MS results



- initial material identified as $3\text{UO}_3 \cdot 2\text{NH}_3 \cdot 4\text{H}_2\text{O}$ (ADU particles) and $3\text{UO}_3 \cdot \text{NH}_3 \cdot 5\text{H}_2\text{O}$ (ADU powder)
- amorphous phase between 250 °C and 550 °C, for ADU powder $\beta\text{-UO}_3$ reflections at 450 °C and 550 °C
- transition to $\alpha\text{-U}_3\text{O}_8$ for both compounds at 550 °C, completely converted to $\alpha\text{-U}_3\text{O}_8$ at 650 °C
- $m(\text{ADU particles}) = 115.0\%$ (323.0 g mol^{-1}) and $m(\text{ADU powder}) = 116.4\%$ (326.9 g mol^{-1})
- peak for powder from 175 °C to 225 °C (EGA-MS, $\frac{m}{z} = 17$), shoulder for particles starting at ≈ 330 °C

Decomposition of ADU particles and ADU powder in air

Conversion of ADU to UO₃: Decomposition schemes

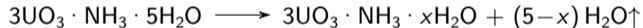
Based on decomposition scheme of 2UO₃ · NH₃ · 3H₂O^a we propose:



up to 200 °C



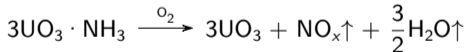
200 °C to 450 °C (3 sub-steps)



up to 175 °C



175 °C to 225 °C

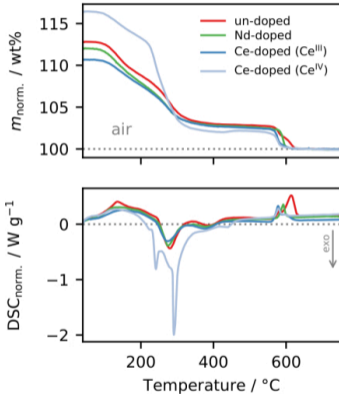


225 °C to 450 °C (2 sub-steps)

^aEloirdi et al. 2014. DOI: 10.1007/s10853-014-8553-0.

Decomposition of *Ln*-doped ADU particles in air

TG-DSC: Calcination in air (un-doped and 10 mol% doped ADU particles, $10\text{ }^\circ\text{C min}^{-1}$)



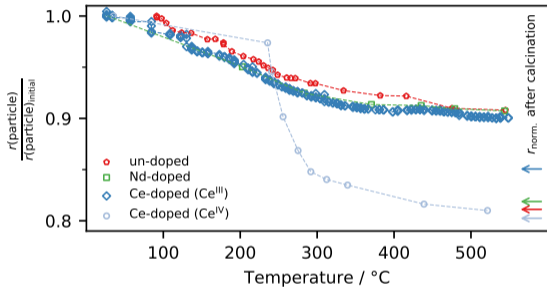
- mass profile and DSC signal of doped compositions prepared with trivalent *Ln* similar to un-doped particles
- huge mass loss observed for Ce-doped particle prepared with Ce^{IV} between $200\text{ }^\circ\text{C}$ to $300\text{ }^\circ\text{C}$, DSC signal indicates at least four exothermic reactions occurring at $241\text{ }^\circ\text{C}$, $259\text{ }^\circ\text{C}$, $275\text{ }^\circ\text{C}$ and $291\text{ }^\circ\text{C}$
- results comparable to TG-DSC data originating from HMTA/urea mixtures \Rightarrow washing ineffective due to amorphous phase

Similar observations were made for CeO_2 particles. A pressurised water treatment was suitable to remove the HMTA/urea residuals^a.

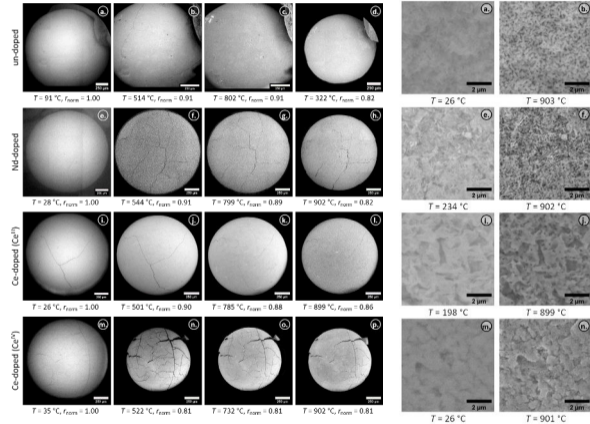
^aKatalenich. 2020. DOI: 10.1007/s10971-020-05230-1.

Decomposition of *Ln*-doped ADU particles in air

In-situ HT-SEM: Calcination in air (un-doped and 10 mol% doped ADU particles, 10 °C min⁻¹)

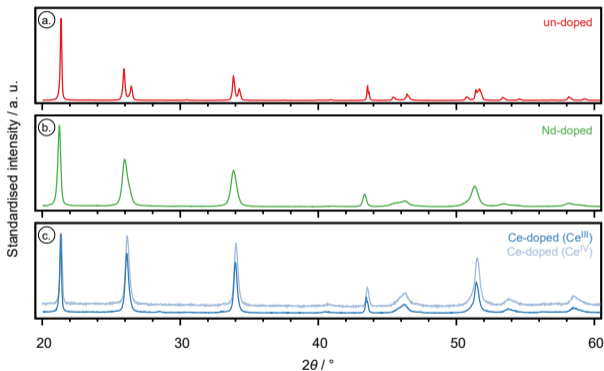


The mass loss goes along with a significant shrinkage and the formation of fragments.



Characterisation of calcination products

XRD: un-doped and *Ln*-doped compositions (10 mol%), calcined in air at 900 °C

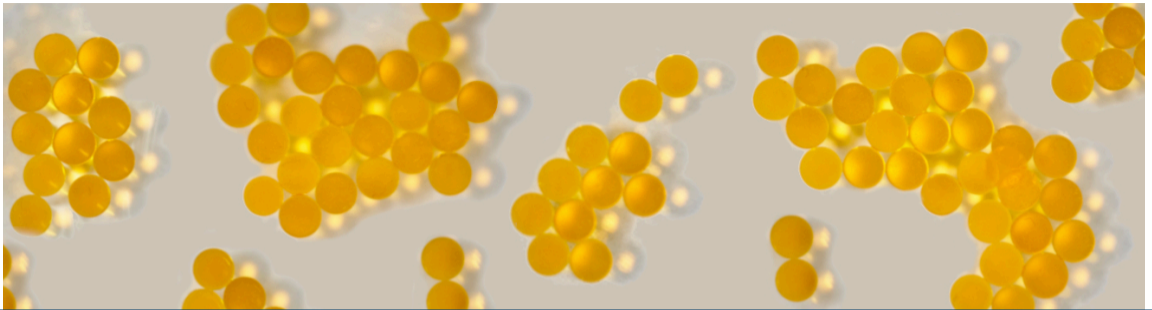


- pattern of **un-doped** particles corresponds to α - U_3O_8 (PDF-2: 01-072-1078)
- comparable pattern obtained for doped compositions \rightarrow *Ln*-doped α - U_3O_8

composition	<i>a</i> / nm	<i>b</i> / nm	<i>c</i> / nm
un-doped	0.41455(1)	1.19549(1)	0.67182(1)
Nd-doped	0.41628(1)	1.19258(2)	0.67552(2)
Ce-doped (Ce ^{III})	0.41519(1)	1.18434(2)	0.67719(2)
Ce-doped (Ce ^{IV})	0.41522(1)	1.18411(2)	0.67644(2)

- determined lattice parameters (*Amm*2) match α - U_3O_8 data^a (*a* = 0.6716 nm, *b* = 1.1960 nm and *c* = 0.4147 nm; *C2mm*)

^aLoopstra. 1964. DOI: 10.1107/S0365110X6400158X.

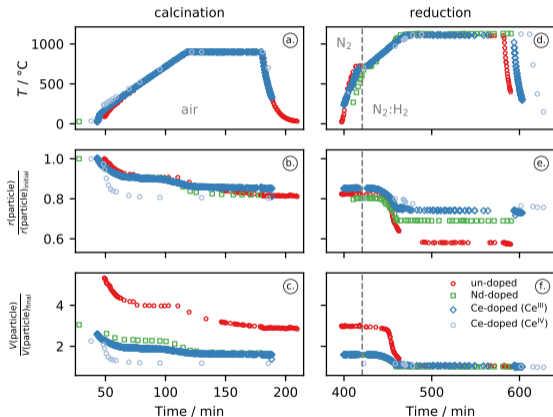
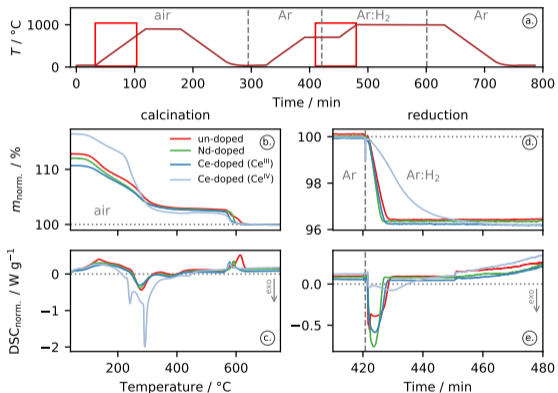


Part IV: Sintering in reducing environment

(ADU particles, *Ln*-doped ADU particles)

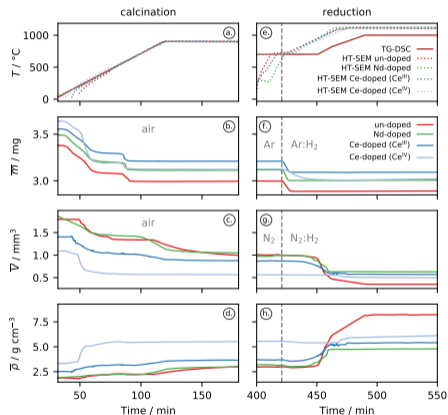
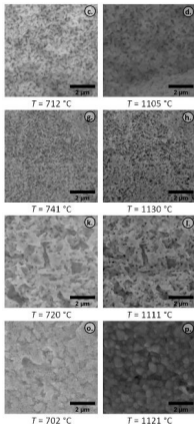
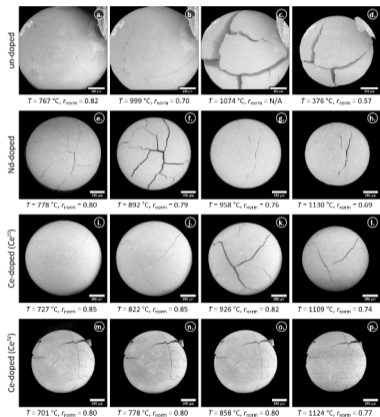
In-situ characterisation during reductive sintering

TG-DSC and HT-SEM results (un-doped and 10 mol% doped ADU particles)



In-situ characterisation during reductive sintering

TG-DSC and HT-SEM results (un-doped and 10 mol% doped ADU particles)



Characterisation of sintered products

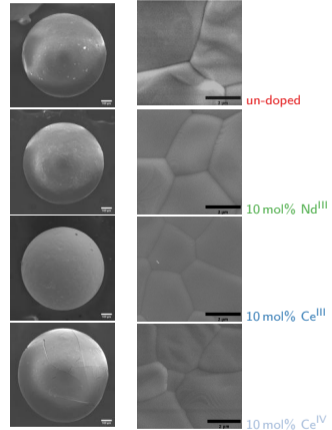
Thermal treatment in high temperature furnace

Calcination in air ($1.5\text{ }^{\circ}\text{C min}^{-1}$, $900\text{ }^{\circ}\text{C}$, 1 h):

- spherical shape maintained for all compositions

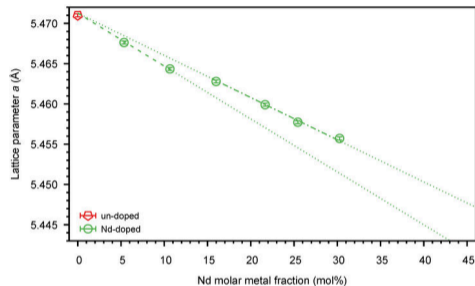
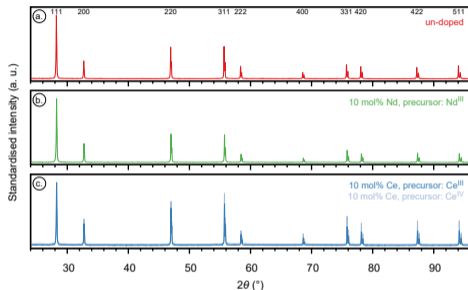
Reduction in Ar:H₂ (99:5, $5\text{ }^{\circ}\text{C min}^{-1}$, $1600\text{ }^{\circ}\text{C}$, 10 h)
with addition of Ar:O₂ (99.5:0.5, $\mu_{\text{O}_2} \approx -420\text{ kJ mol}^{-1}$):

- many broken particles for Ce contents of 20 mol% and 25 mol% prepared with Ce^{III} precursor, for 30 mol% Ce composition only a negligible amount of spheres retained
- particles prepared with Ce^{IV} exhibit cracks on the surface but shrunk less (\rightarrow cracks formed during calcination)
- surface close-ups show neither intergrain nor intragrain pores for all compositions



Characterisation of sintered products

XRD: Lattice parameter of $U_{1-y}Nd_yO_{2\pm x}$ solid solutions



- lattice parameter of $a = 5.4710(2) \text{ \AA}$ determined for **un-doped material**, matching to UO_2 literature lattice parameter ($5.4713(2) \text{ \AA}$)^a

- different charge compensation mechanisms in $U_{1-y}Nd_yO_{2\pm x}$ solid solution^a
 $y < 0.2$: U^V ; $0.2 < y < 0.6$: U^V, U^{VI}, ov ; $y > 0.6$: U^VI

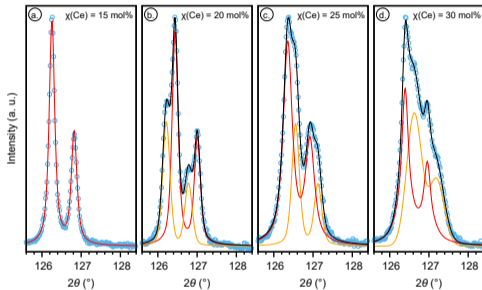
^aLeinders et al. 2015. DOI: 10.1016/j.jnucmat.2015.01.029.

^aBès et al. 2018. DOI: 10.1016/j.jnucmat.2018.04.046.

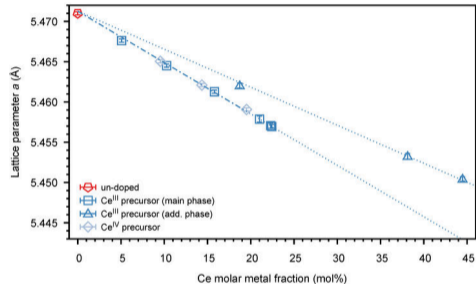
Characterisation of sintered products

XRD: Lattice parameter of $U_{1-y}Ce_yO_{2\pm x}$ solid solutions

026 reflection for compositions with ≥ 15 mol% (Ce^{III} precursor)



- biphasic for $\chi(Ce) \geq 20$ mol% (Ce^{III})
⇒ in agreement with broken particles



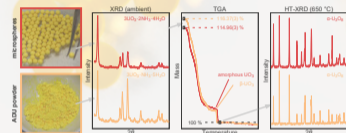
- solubility limit for CeO_2 in UO_2
exceeding ≈ 22 mol% cerium

Conclusions

- Dried un-doped microspheres could be associated to the composition $3\text{UO}_3 \cdot 2\text{NH}_3 \cdot 4\text{H}_2\text{O}$, which converts via amorphous UO_3 into $\alpha\text{-U}_3\text{O}_8$ during calcination in air.
- Nd- and Ce-doped gels with good sphericity and Ln contents up to 30 mol% synthesised, using trivalent Ln precursors, while an incomplete gelation was observed for gels prepared with Ce^{IV} precursors and Ce contents of ≥ 10 mol% with $R = 1.2$ and $c(M)_{\text{sol}} = 1.2 \text{ mol L}^{-1}$.
- $\text{U}_{1-y}\text{Ln}_y\text{O}_{2\pm x}$ single phase solid solutions for sintered Nd- and Ce-doped particles (Ce^{IV} precursor), two solid solutions observed for Ce contents > 15 mol% (Ce^{III} precursor), which relates to the physical stability of those sintered particles (broken particles).
- Amorphous phase in dried gels prepared with Ce^{IV} hinders volatiles to escape the particle during calcination and causes fracturing which leads to surface cracks of the final products.

Journal article

C. Schreinemachers et al.: The conversion of ammonium uranate prepared via sol-gel synthesis into uranium oxides. In: Nuclear Engineering and Technology 52.5 (May 2020), pp. 1013–1021. DOI: 10.1016/j.net.2019.11.004

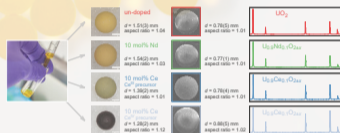


Dataset

C. Schreinemachers and G. Leinders: Thermal decomposition data of uranium containing microspheres produced via internal gelation and ammonium diuranate powder. (Version 1.0.0) [Data set], License: CC BY-NC-SA. July 2019. DOI: 10.5281/zenodo.3250894

Journal article

C. Schreinemachers et al.: Fabrication of Nd- and Ce-doped uranium dioxide microspheres via internal gelation. In: Journal of Nuclear Materials 535 (July 2020), p. 152128. DOI: 10.1016/j.jnucmat.2020.152128

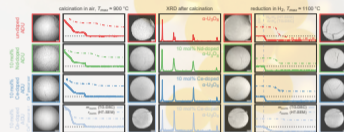


Dataset

C. Schreinemachers and G. Leinders: Characterisation data of Nd- and Ce-doped uranium dioxide microspheres prepared via internal gelation. (Version 1.0.0) [Data set], License: CC BY-NC. 2020. DOI: 10.5281/zenodo.3560620

Journal article

C. Schreinemachers et al.: Structural changes of Nd- and Ce-doped ammonium diuranate microspheres during the conversion to U_{1-y}Ln_yO_{2±x}. In: Journal of Nuclear Materials 542 (Dec. 2020), p. 152454. DOI: 10.1016/j.jnucmat.2020.152454



Dataset

C. Schreinemachers et al.: HT-SEM data of un-doped, Nd-doped and Ce-doped ammonium diuranate microspheres during the conversion to (Ln-doped) uranium dioxide. in preparation. DOI: 10.5281/zenodo.3745551

Acknowledgements

- Dr. Václav Tyrpekl (Charles University, Prague)
- Dr. Frédéric Jutier (SCK CEN)
- Koen Vanaken (SCK CEN)
- Peter Dries (SCK CEN)
- Eddy Kox (SCK CEN)
- Olivier Bollen (KU Leuven)
- Joseph Lautru (ICSM, CNRS)

GENIORS

GEN IV integrated oxide fuels recycling strategies

The GENIORS project received funding from the
H2020 Euratom Research and Innovation Programme
(grant agreement n°755171)



economie

FOD Economie, K.M.O., Middenstand en Energie

project: ASOF - Advanced Separation for
Optimal management of spent Fuel

sck cen Academy

References I



Bès, R. et al.: New insight in the uranium valence state determination in $U_yNd_{1-y}O_{2\pm x}$. In: Journal of Nuclear Materials 507 (Aug. 2018), pp. 145–150. ISSN: 0022-3115. DOI: 10.1016/j.jnucmat.2018.04.046.



Chevalier, P.-Y. et al.: Progress in the thermodynamic modelling of the O–U binary system. In: Journal of Nuclear Materials 303.1 (May 2002), pp. 1–28. DOI: 10.1016/s0022-3115(02)00813-9.



Collins, J. L. et al.: The basic chemistry involved in the internal-gelation method of precipitating uranium as determined by pH measurements. In: Radiochimica Acta 42.3 (1987), pp. 121–134. DOI: 10.1524/ract.1987.42.3.121.



Cordfunke, E. H. P.: On the uranates of ammonium – I: The ternary system $NH_3 - UO_3 - H_2O$. In: Journal of Inorganic and Nuclear Chemistry 24.3 (1962), pp. 303–307. ISSN: 0022-1902. DOI: 10.1016/0022-1902(62)80184-5.



Debets, P. C. and B. O. Loopstra: On the uranates of ammonium – II: X-ray investigation of the compounds in the system $NH_3 - UO_3 - H_2O$. In: Journal of Inorganic and Nuclear Chemistry 25.8 (1963), pp. 945–953. ISSN: 0022-1902. DOI: 10.1016/0022-1902(63)80027-5.

References II



Eloirdi, R. et al.: Investigation of ammonium diuranate calcination with high-temperature X-ray diffraction. In: Journal of Materials Science 49.24 (2014), pp. 8436–8443. ISSN: 1573-4803. DOI: 10.1007/s10853-014-8553-0.



Guéneau, C. et al.: Thermodynamic modelling of advanced oxide and carbide nuclear fuels: Description of the U–Pu–O–C systems. In: Journal of Nuclear Materials 419.1-3 (Dec. 2011), pp. 145–167. DOI: 10.1016/j.jnucmat.2011.07.033.



Higgs, J. D. et al.: A conceptual model for the fuel oxidation of defective fuel. In: Journal of Nuclear Materials 366.1-2 (June 2007), pp. 99–128. DOI: 10.1016/j.jnucmat.2006.12.050.



Katalenich, J. A.: Use of a pressurized water treatment to prevent cracking of internal gelation sol-gel microspheres. In: Journal of Sol-Gel Science and Technology 94.2 (Mar. 2020), pp. 298–309. DOI: 10.1007/s10971-020-05230-1.



Labroche, D. et al.: Thermodynamics of the O – U system. I – Oxygen chemical potential critical assessment in the UO_2 – U_3O_8 composition range. In: Journal of Nuclear Materials 312.1 (Jan. 2003), pp. 21–49. DOI: 10.1016/S0022-3115(02)01322-3.



Leinders, G. et al.: Accurate lattice parameter measurements of stoichiometric uranium dioxide. In: Journal of Nuclear Materials 459 (2015), pp. 135–142. ISSN: 0022-3115. DOI: 10.1016/j.jnucmat.2015.01.029.

References III



Lindemer, T. B. and T. M. Besmann: Chemical thermodynamic representation of $\text{UO}_{2\pm x}$. In: Journal of Nuclear Materials 130 (1985), pp. 473–488. ISSN: 0022-3115. DOI: 10.1016/0022-3115(85)90334-4.



Loopstra, B. O.: Neutron diffraction investigation of U_3O_8 . In: Acta Crystallographica 17.6 (June 1964), pp. 651–654. DOI: 10.1107/S0365110X6400158X.



Lundberg, D. and I. Persson: The size of actinoid (III) ions—structural analysis vs. common misinterpretations. In: Coordination Chemistry Reviews 318 (2016), pp. 131–134. DOI: 10.1016/j.ccr.2016.04.003.



Schreinemachers, C. and G. Leinders: Characterisation data of Nd- and Ce-doped uranium dioxide microspheres prepared via internal gelation. (Version 1.0.0) [Data set], License: CC BY-NC. 2020. DOI: 10.5281/zenodo.3560620.



Schreinemachers, C. and G. Leinders: Thermal decomposition data of uranium containing microspheres produced via internal gelation and ammonium diuranate powder. (Version 1.0.0) [Data set], License: CC BY-NC-SA. July 2019. DOI: 10.5281/zenodo.3250894.



Schreinemachers, C. et al.: Fabrication of Nd- and Ce-doped uranium dioxide microspheres via internal gelation. In: Journal of Nuclear Materials 535 (July 2020), p. 152128. DOI: 10.1016/j.jnucmat.2020.152128.

References IV



Schreinemachers, C. et al.: HT-SEM data of un-doped, Nd-doped and Ce-doped ammonium diuranate microspheres during the conversion to (*Ln*-doped) uranium dioxide. in preparation. DOI: 10.5281/zenodo.3745551.



Schreinemachers, C. et al.: Structural changes of Nd- and Ce-doped ammonium diuranate microspheres during the conversion to $U_{1-y}Ln_yO_{2\pm x}$. In: Journal of Nuclear Materials 542 (Dec. 2020), p. 152454. DOI: 10.1016/j.jnucmat.2020.152454.



Schreinemachers, C. et al.: The conversion of ammonium uranate prepared via sol-gel synthesis into uranium oxides. In: Nuclear Engineering and Technology 52.5 (May 2020), pp. 1013–1021. DOI: 10.1016/j.net.2019.11.004.



Shannon, R. D.: Revised effective ionic radii and systematic studies of interatomic distances in halides and chalcogenides. In: Acta Crystallographica Section A 32.5 (Sept. 1976), pp. 751–767. DOI: 10.1107/S0567739476001551.